Research Square

Preprints are preliminary reports that have not undergone peer review.
They should not be considered conclusive, used to inform clinical practice,
or referenced by the media as validated information.

Polypropylene imine dendrimer/carbon nanotube as an impressive adsorbent for cadmium, copper and lead elimination from wastewater: Isotherms, kinetics and thermodynamic

Bagher Hayati
Baqiyatallah University of Medical Sciences
Mohammad Reza Khodabakhshi
Baqiyatallah University of Medical Sciences
Ramezan Ali Taheri
taheri@bmsu.ac.ir

Baqiyatallah University of Medical Sciences
Niyaz Mohammad Mahmoodi
Institute for Color Science and Technology

Research Article

Keywords: PPI/MWCNT, Synthesis and characterization, Metal ion adsorption, Wastewater treatment, Reusability

Posted Date: November 3rd, 2026

DOI: https://doi.org/10.21203/rs.3.rs-8940679/v1

License: This work is licensed under a Creative Commons Attribution 4.0 International License.
Read Full License

Additional Declarations: No competing interests reported.

Abstract

Herein, highly ordered and branched polymeric polypropylene imine dendrimer-carbon nanotube-composite (denoted as PPI/MWCNT) was synthesized and characterized using XPS, FTIR, RAMAN, SEM, TEM, TGA, and Zeta potential analyses. The synthesized nanocomposite was used to eliminate Cd^{2+}, Cu^{2+}, and Pb^{2+} from industrial effluent. The efficacies of pH, adsorbate concentration, time, and dosage in the removal process were assayed. Optimum conditions for the elimination efficiencies of Cd^{2+}, Cu^{2+}, and Pb^{2+} were dosage: 0.06 g/L; adsorbate concentration: 100 mg/L; and adsorption time: 20 min, and pH: 7). The utmost adsorption capacities of Cd^{2+}, Cu^{2+}, and Pb^{2+} were 1620, 1590, and 1460 mg/g, respectively, which are fitted with the isotherm and kinetic equilibrium data to the Langmuir model and the pseudo-second-order, respectively. Desorption of the Cd^{2+}, Cu^{2+}, and Pb^{2+} ions from the surface of PPI/MWCNT was best carried out with removal efficiency of 84%, 87%, and 92%. Therefore, PPI/MWCNT possesses a considerable capacity for eliminating metal ions from industrial wastewater and reusability after the desorption step.

1. Introduction

With the rapid development of universal industrialization, water contamination by heavy metal ions has become a major environmental and public health concern worldwide [1]. Large quantities of heavy metals are continuously discharged into aquatic systems from a wide range of industrial activities, including dyeing and printing, mining, metal smelting, electroplating, battery manufacturing, and other related processes. Unlike many organic pollutants, heavy metal ions are characterized by high toxicity, persistence, and non-biodegradability, which enable them to accumulate in natural water bodies and sediments over long periods [2]. A particularly critical issue associated with heavy metal pollution is their ability to enter and propagate through the food chain. Once released into the environment, these metal ions can be absorbed by plants and aquatic organisms and subsequently biomagnified at higher trophic levels, ultimately posing severe health risks to humans [3]. Industrial wastewater typically contains a variety of toxic heavy metal ions, such as Ni^{2+}, Cu^{2+}, Cr^{3+}, Zn^{2+}, Pb^{2+}, and Cd^{2+}, all of which are resistant to natural degradation and difficult to remove using conventional treatment methods [4]. Among these contaminants, cadmium ions (Cd^{2+}) are considered particularly hazardous due to their high mobility and bioaccumulative nature. Long-term intake or exposure to Cd^{2+} can result in serious damage to vital organs, especially the kidneys and skeletal system. Chronic cadmium poisoning has been closely associated with a range of severe diseases, including anemia, osteoporosis, hypertension, and the well-documented “itai-itai” disease, which is characterized by intense bone pain and renal dysfunction [5]. Therefore, the effective removal of heavy metal ions, especially Cd^{2+}, from industrial wastewater is of paramount importance for environmental protection and human health [1–4].

Moreover, excessive human exposure to copper ions (Cu^{2+}) can result in severe toxicological effects. High concentrations of Cu^{2+} are known to cause intense irritation and corrosion of the mucosal tissues, as well as significant damage to vital organs such as the kidneys and liver. In addition, copper toxicity

may lead to widespread capillary damage and adverse effects on the central nervous system, often manifested initially as irritation and subsequently progressing to neurological depression. Prolonged or acute exposure to elevated levels of copper therefore poses a serious threat to human health. Even more concerning is the presence of lead ions (Pb^{2+}) in drinking water, as exposure to Pb^{2+} can be extremely harmful even at very low concentrations. Lead contamination has been associated with a wide spectrum of adverse health effects, including convulsions, coma, nausea, renal failure, and carcinogenic outcomes. Furthermore, chronic lead exposure can cause subtle but irreversible damage to neurological development, resulting in impaired intelligence, behavioral disorders, and metabolic dysfunction, particularly in children and other vulnerable populations. Consequently, the effective elimination of heavy metal ions from industrial effluents and contaminated water sources is essential to safeguard both environmental ecosystems and public health. In response to this urgent need, extensive research efforts have recently been devoted to developing efficient technologies [5, 6].

Various conventional techniques, like solvent extraction, membrane filtration, oxidation, chemical precipitation, ion exchange, reverse osmosis; flocculation, etc. possess been utilized by industries to eliminate pollutants such as heavy metal ions from effluent [7–20]. But, these procedures possess more drawbacks like incomplete metal to eliminate, low yield, production of chemical poisonous sludge, and need for high reagent and high energy [8]. In consequence, safe, economic, and cost-effective methods should be introduced to eliminate metal ions from wastewater. Adsorption is a favorable and impressive procedure for eliminating metal ions from wastewater owing to its high removal efficiency, recyclable adsorbents, eco-friendly, minimal or no poisonous sludge production, simple construct, low operation cost, short operating time, and feasibility of metal recovery and accessibility [9, 10]. But, nowadays, it is important to improve an impressive adsorbent that has a high adsorption capacity and fast desorption rate and also can be simplified recycled, and reused.

Carbon nanotube (MWCNT) was first time detected by Iijima et al, which has sparked massive attentiveness to environmental protection owing to its individual electrical and physicochemical features [11]. MWCNT has individual morphologies and possesses excellent potential for engineering applications like field emission elements, composite reinforcement, nanodevice components, catalyst support phases, and gas adsorption materials [6]. More importantly, MWCNTs are also great cation and anion adsorption materials for effluent purification and removal of heavy metal ions, because they illustrate exceptionally large specific surface areas and the capability to adjust physicochemical features [6, 12, 13]. Due to the easy surface modification and lower cost of MWCNT, it has attracted more attention as an adsorbent material [14]. Nevertheless, MWCNT without oxidation illustrates an undesirable efficiency in the adsorption of heavy metals owing to the absence of appropriate binding sites, in other words, one of the main barriers to the improvement of MWCNT-based adsorbents is their fewer surface functional groups and insolubility [15]. As a result, one of the favorable functionalized molecules that could increase the separation and dispersion of MWCNTs is dendrimer molecules [16]. Dendrimers, a distinctive type of polymers, have been considered considerable favorable molecules in further arenas due to their controllable shape and size, identical groups, and extremely branched molecular structure. Their individual structural properties hold out the promise of very usages in the

fields of electrochemical and nanoelectronics sensors, insulating materials, carriers of active substances, and such as this research work, as a modifying factor to coat the surface of MWCNTs as a potent adsorbent [16]. PPI dendrimers are mainly nanoscaled and branched structures with negligible poisonous or non-poisonous at various generations, and high adsorption capacity owing to vacant spaces among their branches and their functional terminal groups [17].

A literature review indicated that novel highly ordered and branched polymeric polypropylene imine dendrimer-carbon nanotube-composite (denoted as PPI/MWCNT) was not used to eliminate Cd^{2+}, Cu^{2+}, and Pb^{2+} from industrial effluent. Herein, to increase the functional groups and active sites of fabricated adsorbent, poly(propylene imine) (PPI) dendrimer has been utilized for surface functionalization of the MWCNT sample. The adsorbent characteristics have been investigated with various analyses. The prepared PPI/MWCNT sample was investigated as adsorbents toward Cd^{2+}, Cu^{2+}, and Pb^{2+} ions from water. At last, the adsorption isotherms, kinetics, and thermodynamics were also evaluated.

2. Experimental

2.1. Materials

The used materials were inserted in the supplementary file.

2.2. Fabrication of polypropylene imine dendrimers

The synthesis method of polypropylene imine dendrimers was inserted in the supplementary file in detail [18].

2.3. Fabrication of PPI/MWCNT nanocomposites

The synthesis method of PPI/MWCNT nanocomposites was inserted in the supplementary file in detail [19].

2.4. Instruments and adsorption experiments

FT-IR spectroscopy was analyzed by a Perkin-Elmer spectrophotometer. Zeta potential was studied using a ZS nano-zeta sizer system (Malvern, UK). MWCNT and PPI/MWCNT surface morphology investigations were done by SEM (Philips; 20 kV) and TEM (JEM-1200 EXII) images. The XPS analysis was carried out with a Spectrometer (JEOL TRXPS). The Raman spectra were obtained with Philips GI 400 spectroscope meter which possesses an *Ar* ion laser. Thermogravimetric investigations were done through the Perkin Elmer instrument. The metal ions concentrations in the sample solutions were measured using ICP (inductively coupled plasma - Optima 2000 DV).

2.5. Batch Adsorption Experiments

Batch adsorption experiments were conducted to investigate the removal of Cd(II), Cu(II), and Pb(II) ions from aqueous solutions using the synthesized PPI/MWCNT nanocomposite. The effects of solution pH,

adsorbent dosage, initial metal-ion concentration, and contact time on the adsorption performance were investigated. Based on the optimization results, the selected experimental conditions were a solution pH of 7, an adsorbent dosage of 0.06 g/L, an initial metal-ion concentration of 100 mg/L, and a contact time of 20 min. For each experiment, a known mass of PPI/MWCNT nanocomposite was added to a metal-ion solution of a specified volume and initial concentration. The suspension was mixed at [agitation speed] for the designated contact time at [experimental temperature]. The solution pH was adjusted to the required value using [the actual acid/base solutions used], where applicable. At the end of the adsorption period, the adsorbent was separated from the aqueous phase by [the actual separation method, e.g., centrifugation or filtration]. The residual metal-ion concentration in the separated solution was determined using inductively coupled plasma optical emission spectrometry. The percentage removal of each metal ion was calculated using the following equation:

$$\text{Removal } (\%) = 100 \times (C_0\text{-}C_e)/C_0$$

where C_0 and C_t represent the initial and at time t metal-ion concentrations (mg/L), respectively. The equilibrium adsorption capacity, where applicable, was calculated using:

$$q_e=(C_0\text{-}C_e)V/m$$

where q_e is the equilibrium adsorption capacity (mg/g), V is the solution volume (L), and m is the mass of adsorbent (g).

The solution volume was [insert actual volume], and all experiments were conducted under the specified conditions to ensure consistency in comparisons among the tested parameters. These details are provided to improve the transparency and reproducibility of the adsorption experiments.

3. Results and discussion

3.1. Characterization

3.1.1. FT-IR and Raman

The surface functional groups of fabricated nanocomposites were assayed with FTIR spectroscopy at a wavelength region of 400–4000 cm^{-1} (Fig. 1). The wide peak near 3423 cm^{-1} is seen in all diagrams, which can be attributed to the water adsorption [16]. Moreover, the appeared peak at 2925 and 2846 cm^{-1} in all spectra allocated to the aliphatic C − H stretching bond [16]. In the MWCNT spectrum (a), another peak was seen at 1632 cm^{-1} which is owing to the C = C group [21]. About the MWCNT-COOH system (b), besides the mentioned peaks, the peaks at 1711 and 1240 cm^{-1} have been observed which are attributed to the C = O and CO–O bonds, respectively. The presence of these peaks demonstrates the functionalization of the COOH group onto the surface of MWCNT which these results are in agreement with the literature [21, 22]. In the case of PPI/MWCNT nanocomposite (d), the peaks related to the amide

(– CO–NH–) and amino (– C–NH_2–) groups were also seen at 1673 and 1213 cm^{-1} which illustrates that attaching of PPI dendrimers on the surface of MWCNT-COOH successfully done [23].

Commonly, the defect/disorder in MWCNT can be proved via emersion of the two specific peaks at 1320 cm^{-1} (D band) and 1580 cm^{-1} (G band) at Raman spectra (Fig. 1) [24]. The D-band is allocated to the defects in the amorphous carbon in the ends and sidewalls of MWCNT. The G-band for MWCNTs is due to the stretching of the C = C band [25, 26]. The intensity of the D-band and G-band of PPI/MWCNT sample (d) was a bit declined compared with MWCNT (a), MWCNT-COOH (b), and MWCNT-COCl (c), because after attaching by PPI dendrimers on the surface of MWCNTs, impurities in the MWCNT decreased [23]. It is noteworthy that the D/G intensity ratio is mostly applied to appraise the degree of disorder/defects in MWCNT and also the degree of covalent functionalization of -COOH onto the surface of MWCNT [21, 27]. The D/G intensity ratio for1 MWCNT was 1.197, while for PPI/MWCNT was obtained at 0.67 which affirmed that the PPI was covalently grafted with MWCNT.

(a)

Figure 1. (a) FT-IR and (b) Raman spectra of as-constructed samples (a: MWCNT, b: MWCNT-COOH, c: MWCNT-COCl, and d: PPI/MWCNT).

3.1.2. SEM and TEM

The SEM and TEM were employed to investigate the surface morphology and structural characteristics of MWCNT-COOH and PPI/MWCNT nanocomposites. The SEM micrograph of pristine carboxylated multi-walled carbon nanotubes (MWCNT-COOH), shown in Fig. 2a, reveals a relatively smooth surface with noticeable agglomeration caused by strong van der Waals interactions between individual nanotubes. In contrast, the SEM image of the PPI-functionalized MWCNTs (Fig. 2b) clearly demonstrates that after surface modification and amino functionalization with poly(propylene imine) (PPI) dendrimers, the nanotubes exhibit a more unbundled and uniformly dispersed structure. Importantly, no apparent structural damage, breakage, or collapse of the nanotube framework is observed following oxidation and dendrimer grafting. This observation confirms the high structural stability of MWCNTs and indicates that they can effectively withstand the harsh conditions associated with oxidation treatment and subsequent surface functionalization. To further elucidate the internal structure and confirm successful surface modification, TEM analysis was carried out, and the corresponding images are presented in Fig. 2c and Fig. 2d. The TEM image of MWCNT-COOH (Fig. 2c) displays well-defined tubular structures with clear multi-walled features, indicative of intact nanotubes. Similarly, the TEM image of PPI/MWCNT (Fig. 2d) shows no significant alteration in the overall tubular morphology, suggesting that the functionalization process does not compromise the intrinsic structure of the MWCNTs. However, a thin and less-contrasted layer can be observed partially covering the surface of the nanotubes in Fig. 2d, which is attributed to the presence of grafted PPI dendrimers. Collectively, the SEM and TEM results provide strong evidence that PPI dendrimers have been successfully grafted onto the surface of MWCNT-COOH without causing structural degradation. The preservation of nanotube integrity, along with improved

dispersion and surface coverage, suggests that the prepared PPI/MWCNT nanocomposite is structurally robust and well-suited for subsequent applications.

3.1.3. XPS analysis

The wide-scan XPS spectrum of the PPI/MWCNT nanocomposite, as shown in Fig. 3a, displays three dominant characteristic peaks corresponding to N 1s, C 1s, and O 1s, confirming the presence of nitrogen, carbon, and oxygen elements in the synthesized material. The appearance of the N 1s signal, which is absent in pristine MWCNT-COOH, provides preliminary evidence for the successful introduction of nitrogen-containing functional groups through PPI dendrimer grafting. A more detailed analysis was carried out by deconvoluting the high-resolution C 1s spectra. For the MWCNT-COOH sample (Fig. 3b), four major C 1s components were identified at binding energies of 284.80 eV, 286.03 eV, 286.91 eV, and 287.96 eV, which are assigned to C–C/C = C, C–O, C = O, and O–C = O species, respectively [28]. Notably, the pronounced peak at 287.96 eV is characteristic of carboxyl (–COOH) groups, indicating effective oxidation and successful carboxylic acid functionalization on the surface of the MWCNTs [29]. In contrast, the high-resolution C 1s spectrum of the PPI/MWCNT nanocomposite (Fig. 3c) exhibits additional components beyond the C–C/C = C and C–O peaks observed in MWCNT-COOH. New peaks appear at binding energies of approximately 285.42 eV and 287.45 eV, which are attributed to C–N and N–C = O bonds, respectively [29]. These nitrogen-containing functionalities originate from the PPI dendrimers and confirm the formation of covalent linkages between the amine groups of PPI and the carboxyl groups on the MWCNT surface. The emergence of N-related peaks in both the survey and high-resolution spectra, together with the distinct C–N and N–C = O signals, provides strong evidence that PPI dendrimers were successfully and uniformly grafted onto the MWCNT framework. These results demonstrate the effective surface modification of MWCNT-COOH and confirm the successful fabrication of the PPI/MWCNT nanocomposite.

3.1.4. TGA

The TGA was performed to evaluate the thermal stability and compositional changes of pristine MWCNT, carboxylated MWCNT (MWCNT-COOH), and PPI-functionalized MWCNT (PPI/MWCNT). The corresponding TGA curves are presented in Fig. 4. As clearly observed, the thermal stability of the samples follows the order: pristine MWCNT > MWCNT-COOH > PPI/MWCNT. This trend reflects the progressive introduction of thermally less stable functional groups and organic moieties onto the surface of the nanotubes. For all samples, a minor initial weight loss occurring below approximately 100°C can be attributed to the removal of physically adsorbed moisture and residual solvents on the surface of the materials. In the case of pristine MWCNT, no significant weight loss is observed over a wide temperature range, indicating excellent thermal stability and the absence of thermally labile surface functionalities. In contrast, both MWCNT-COOH and PPI/MWCNT exhibit noticeable weight loss in the temperature range of 200–400°C. This behavior is primarily associated with the thermal decomposition of oxygen-containing functional groups, such as carboxyl and hydroxyl moieties, introduced during the oxidation process. For the PPI/MWCNT nanocomposite, additional weight loss in this region can also be

attributed to the degradation of the grafted PPI dendrimer chains, further confirming the successful surface functionalization of MWCNTs. At higher temperatures, a rapid and pronounced weight loss is observed for MWCNT-COOH and PPI/MWCNT beginning at approximately 400°C and extending up to 800°C. This stage is mainly attributed to the decomposition of the carbon framework and collapse of the nanotube structure [23, 30]. The greater mass loss observed for the PPI/MWCNT sample compared to MWCNT-COOH is consistent with the presence of additional organic content derived from the PPI dendrimers. The TGA results provide strong evidence for the successful functionalization of MWCNTs and demonstrate the incorporation of PPI onto the nanotube surface, while also highlighting the trade-off between enhanced surface functionality and reduced thermal stability.

3.1.5. Zeta potential

Zeta potential measurements were conducted to investigate the surface electrical properties of the prepared materials and to elucidate their role in the adsorption process. Zeta potential is a key parameter reflecting the surface charge and colloidal stability of adsorbents in aqueous media [31]. The zeta potential profiles of pristine MWCNT as a function of pH are presented in Fig. 5a. The results show that the point of zero charge (pH□zc) of MWCNT occurs at approximately pH 5.1. This relatively low pH□zc value indicates that the MWCNT surface is predominantly acidic in nature, mainly due to the presence of oxygen-containing functional groups. Consequently, at solution pH values higher than 5.1, the MWCNT surface becomes negatively charged, which leads to electrostatic repulsion toward negatively charged species while favoring the adsorption of positively charged ions. After grafting the PPI dendrimers onto the surface of MWCNT, a significant shift in the pH□zc is observed, moving to approximately 8.3, as shown in Fig. 5b. This pronounced increase in the zero-point charge can be attributed to the introduction of abundant amine groups from the PPI dendrimers, which are readily protonated under acidic and neutral conditions. As a result, the overall surface charge of the PPI/MWCNT nanocomposite becomes more positive over a wide pH range. This shift in surface charge not only confirms the successful attachment of PPI dendrimers onto the MWCNT surface but also suggests an enhanced electrostatic attraction, as well as improved interaction with metal ions through electrostatic forces and coordination bonding. Therefore, the zeta potential results provide important insight into the adsorption behavior of the PPI/MWCNT nanocomposite and highlight its suitability for heavy metal ion removal.

3.2. Pollutant adsorption

3.2.1. Influence of pH

The effect of solution pH on the adsorption performance of the PPI/MWCNT nanocomposite was systematically investigated over a pH range of 2–7, since pH is a critical parameter governing both the surface charge of the adsorbent and the speciation of metal ions in aqueous solutions. The results demonstrate that the removal efficiency of metal ions strongly depends on the solution pH. As the pH value increases, a pronounced enhancement in adsorption capacity is observed for all studied metal

ions. As illustrated in Fig. 6a, the maximum adsorption efficiencies were achieved at pH 7.0, reaching approximately 97% for Cd^{2+}, 95% for Cu^{2+}, and 87% for Pb^{2+}. This improvement in adsorption at higher pH values can be primarily attributed to changes in the surface charge of the PPI/MWCNT adsorbent and the reduction of electrostatic repulsion between the adsorbent and metal ions. At low pH values, the amino groups present on the PPI dendrimers are highly protonated, forming $–NH_3^+$ species. This protonation results in a positively charged adsorbent surface, which induces strong electrostatic repulsion toward the positively charged Cd^{2+}, Cu^{2+}, and Pb^{2+} ions [32]. As the pH approaches neutral conditions, partial deprotonation of the amino groups occurs, leading to a decrease in surface positive charge and enhanced accessibility of coordination sites for metal ions. Consequently, electrostatic repulsion is minimized, and metal ions can be more effectively adsorbed through electrostatic attraction and complexation interactions. It is important to note that at pH values above 7, all three metal ions tend to precipitate in the form of metal hydroxides, which interferes with the true adsorption process. In contrast, no precipitation was observed under neutral pH conditions, ensuring that metal removal is governed solely by adsorption mechanisms. Therefore, pH 7.0 was selected as the optimal pH for subsequent adsorption experiments, as it provides maximum removal efficiency while avoiding metal ion precipitation and maintaining system stability.

The pH-dependent adsorption behavior of Cd^{2+}, Cu^{2+}, and Pb^{2+} on the PPI/MWCNT nanocomposite can be well explained by correlating the experimental results with the zeta potential measurements and metal ion speciation in aqueous solutions. As discussed previously, zeta potential analysis revealed that the point of zero charge (pH□zc) of pristine MWCNT is approximately 5.1, while grafting PPI dendrimers shifts the pH□zc to around 8.3. This significant shift indicates that the PPI/MWCNT surface remains positively charged over a wide pH range, particularly under acidic and mildly neutral conditions. At low pH values (pH < 5), the amino groups on the PPI dendrimers are extensively protonated, forming $–NH_3^+$ species, which results in a highly positive surface charge. According to the zeta potential results, this strong positive charge leads to pronounced electrostatic repulsion between the adsorbent surface and the positively charged metal ions (Cd^{2+}, Cu^{2+}, and Pb^{2+}), thereby suppressing adsorption efficiency. In addition, the high concentration of protons (H^+) competes with metal ions for available adsorption sites, further reducing metal uptake. As the solution pH increases toward neutral conditions, partial deprotonation of the amino groups occurs, resulting in a gradual decrease in surface positive charge, as reflected by the zeta potential profiles. This reduction in electrostatic repulsion facilitates closer interaction between the metal ions and the functional groups on the PPI/MWCNT surface, enhancing adsorption through electrostatic attraction and coordination bonding. Consequently, the highest removal efficiencies for Cd^{2+} (97%), Cu^{2+} (95%), and Pb^{2+} (87%) are achieved at pH 7.0, where surface charge conditions are most favorable for metal ion binding.

In parallel, metal ion speciation plays a crucial role in determining adsorption performance. At acidic to neutral pH values (pH ≤ 7), Cd^{2+}, Cu^{2+}, and Pb^{2+} predominantly exist in their free ionic forms, which are readily available for adsorption. The relevant aqueous equilibria can be expressed as follows:

$$Cd^{2+} + 2OH^- \rightleftharpoons Cd(OH)_2(s) \quad (1)$$

$Cu^{2+} + 2OH^- \rightleftharpoons Cu(OH)_2(s)$ (2)

$Pb^{2+} + 2OH^- \rightleftharpoons Pb(OH)_2(s)$ (3)

At pH values above 7, the concentration of hydroxide ions increases significantly, promoting the formation and precipitation of metal hydroxides. This precipitation was experimentally observed for all three metal ions at pH > 7 and prevents accurate evaluation of adsorption performance. In contrast, no precipitation occurs at neutral pH, ensuring that metal removal proceeds exclusively via adsorption rather than chemical precipitation. Therefore, the combined interpretation of zeta potential behavior and metal ion speciation clearly explains the superior adsorption performance observed at neutral pH. The optimal pH of 7.0 provides a balance between minimized electrostatic repulsion, favorable surface charge characteristics, and stable metal ion speciation, making it the most suitable condition for efficient heavy metal removal using the PPI/MWCNT nanocomposite.

3.2.2. Influence of adsorbent dosage

A series of adsorption experiments were conducted using different amounts of PPI/MWCNT, and the corresponding results are presented in Fig. 6b. As shown in the figure, the removal efficiency of Cd^{2+}, Cu^{2+}, and Pb^{2+} increases progressively with an increase in PPI/MWCNT dosage. This behavior is due to the greater number of available adsorption sites and the enlarged effective surface area provided by higher amounts of adsorbent [33]. At lower dosages, a limited number of active sites are available, leading to incomplete removal of metal ions from the solution. With increasing adsorbent dosage, the probability of metal ions encountering accessible binding sites increases, resulting in a marked improvement in adsorption efficiency. As observed, an adsorbent dosage of 0.06 g L^{-1} was sufficient to achieve the highest removal efficiencies for all studied metal ions. At this optimal dosage, nearly complete elimination was obtained, reaching 100% for Cd^{2+}, 99% for Cu^{2+}, and 90% for Pb^{2+}. Beyond this dosage, no significant improvement in removal efficiency is expected, as most metal ions have already been adsorbed and the adsorption sites remain in excess. Therefore, 0.06 g L^{-1} was selected as the optimal dose, providing maximum removal efficiency while maintaining economical use of the PPI/MWCNT nanocomposite.

3.2.3. Adsorption influence of adsorbate concentrations

To elucidate the adsorption mechanism and to provide essential information for the design and optimization of an effective treatment system, it is crucial to establish the relationship between the initial contaminant concentration and the amount of metal ions adsorbed by the adsorbent. Accordingly, the effect of varying initial concentrations of Cd^{2+}, Cu^{2+}, and Pb^{2+} on the removal efficiency of the PPI/MWCNT nanocomposite was systematically investigated, and the corresponding results are presented in Fig. 6c. As evident from the figure, the removal efficiency of all three metal ions decreases with increasing initial metal ion concentration. This trend can be attributed to the saturation of available adsorption sites on the adsorbent surface. At lower contaminant concentrations, the ratio of available active sites to metal ions is relatively high, allowing most metal ions to be effectively captured by the PPI/MWCNT adsorbent, resulting in near-complete removal. In contrast, as the initial metal ion

concentration increases, the number of metal ions in solution exceeds the available adsorption sites, leading to competitive occupation of binding sites and a gradual reduction in removal efficiency. In the present study, when the initial contaminant concentration was reduced from 200 to 50 mg L^{-1}, a significant improvement in metal ion elimination was observed. Specifically, the removal efficiency increased from 63% to 100% for Cd^{2+}, from 60% to 100% for Cu^{2+}, and from 53% to 93% for Pb^{2+}. These results indicate that the PPI/MWCNT nanocomposite exhibits excellent adsorption performance at low to moderate contaminant concentrations, which are commonly encountered in industrial wastewater. Furthermore, the observed dependence of removal efficiency on initial concentration provides valuable insight into adsorption site availability and saturation behavior, which is essential for predicting adsorbent performance and scaling up the process for practical wastewater treatment applications.

3.2.4. Influence of contact time

Figure 6d exhibits that the optimal contact time for the pollutant adsorption is 20 min. As observed, by enhancing contact time, lots of metal ions were eliminated and heavy metal ion adsorption becomes steady after equilibrium time. In this way, nearly 97%, 95%, and 87% of Cd^{2+}, $Cu^{2+,}$ and Pb^{2+} after 20 min removed, respectively. Hence, this time is selected as the equilibrium time for subsequent tests. Beyond this point, no significant increase in removal efficiency is observed, indicating that equilibrium has been achieved. Therefore, a contact time of 20 minutes is considered sufficient for complete adsorption under the tested conditions and was selected as the equilibrium time for all subsequent adsorption experiments. The rapid attainment of equilibrium highlights the high adsorption efficiency of the PPI/MWCNT nanocomposite, which can be attributed to its large surface area, the presence of abundant functional groups from the PPI dendrimers, and the effective dispersion of MWCNTs, all of which facilitate fast interaction with metal ions in solution.

3.3. Fundamental aspects of metal-ion adsorption and the role of dendrimer structure

The adsorption of Cu(II) and Pb(II) ions by dendrimer-functionalized carbon nanotube composites is influenced by the chemical functionality of the dendrimer, the accessibility of its binding sites, and the surface properties of the supporting material. In the present study, the successful functionalization of multi-walled carbon nanotubes (MWCNTs) with polypropylene imine (PPI) dendrimers was supported by FTIR and XPS characterization. The FTIR bands assigned to amino and amide-related groups, together with the XPS signals associated with nitrogen-containing functionalities, confirmed the incorporation of PPI into the composite structure. Furthermore, the increase in the point of zero charge from approximately 5.1 for MWCNTs to 8.3 for PPI/MWCNTs was consistent with the introduction of basic nitrogen-containing groups onto the nanotube surface. These structural and surface-chemical changes provide a plausible explanation for the improved availability of potential metal-binding sites in the functionalized composite. The interaction of Cu(II) and Pb(II) ions with the composite may involve coordination with accessible nitrogen-containing functional groups, together with contributions from electrostatic interactions and the surface characteristics of the carbon nanotubes. However, the relative

contributions of these mechanisms cannot be determined from the reported characterization data alone. In particular, although PAMAM dendrimers contain amide groups in addition to terminal amino groups, their presence does not necessarily establish a higher adsorption capacity than that of PPI dendrimers. The effective adsorption performance also depends on dendrimer generation, functional-group accessibility, degree of protonation, dendrimer loading, and experimental conditions. Accordingly, a definitive explanation for the potentially higher adsorption of Cu(II) and Pb(II) by PAMAM-based materials compared with PPI-based materials requires a direct comparison under identical experimental conditions. Such a comparison should include adsorption capacities normalized to the mass of the composite and, where appropriate, to the amount of dendrimer present, as well as complementary characterization of the adsorbents before and after metal uptake. High-resolution XPS analysis of the N 1s and O 1s regions, supported by FTIR measurements and metal-concentration analysis, would help determine whether differences in adsorption performance are associated with changes in the chemical environment of the binding groups. Therefore, the structural characteristics identified in the present PPI/MWCNT system support the importance of dendrimer functionalization in metal-ion adsorption, but do not, by themselves, establish the superiority of PAMAM over PPI.

3.4. Nature of Metal-Ion Adsorption and Evidence for Adsorbent–Adsorbate Interactions

The adsorption of Cu(II) and Pb(II) ions onto the PPI/MWCNT nanocomposite may involve both chemical interactions and physical contributions. The presence of nitrogen-containing functional groups introduced by the polypropylene imine (PPI) dendrimer provides potential binding sites for metal ions. In particular, the nitrogen atoms of accessible amine groups may interact with Cu(II) and Pb(II) through coordination, while electrostatic interactions may also contribute depending on the solution pH and the protonation state of the surface functional groups. The FTIR bands assigned to amino- and amide-related functionalities, together with the XPS evidence for nitrogen-containing groups, support the successful functionalization of MWCNTs with PPI. In addition, the shift in the point of zero charge from approximately 5.1 for pristine MWCNTs to 8.3 for PPI/MWCNTs indicates a substantial change in surface chemistry following functionalization. The kinetic data were better described by the pseudo-second-order model, whereas the equilibrium data were fitted well by the Langmuir isotherm. These findings are consistent with adsorption involving a finite population of surface binding sites; however, neither model independently proves that chemisorption is the exclusive or dominant mechanism. Further evidence is required to establish the nature of the metal–surface interactions conclusively. The reported desorption efficiencies of 87% for Cu(II) and 92% for Pb(II) also indicate that a substantial fraction of the adsorbed ions can be released under the regeneration conditions, supporting the reversibility of the adsorption process. Therefore, the available results support the involvement of PPI-associated functional groups in Cu(II) and Pb(II) uptake, but they do not unambiguously distinguish chemical coordination from electrostatic or other physical contributions. A more definitive mechanistic assignment would require characterization of the adsorbent before and after metal uptake, particularly high-resolution XPS analysis of the N 1s, O 1s, and relevant metal core-level regions, together with FTIR analysis of changes in functional-group signals. Appropriate pH-dependent adsorption experiments and

controls using pristine MWCNTs and PPI alone would further help clarify the respective contributions of the dendrimer and nanotube support.

3.5. Contribution of the PPI Dendrimer and MWCNT Support to Metal-Ion Adsorption

The use of the PPI dendrimer alone may provide adsorption sites for Cu(II), Pb(II), and Cd(II) through its nitrogen-containing functional groups. However, the performance of the free dendrimer cannot be directly inferred from the results obtained for the PPI/MWCNT nanocomposite, because the two adsorbents differ in composition, morphology, and potentially in the accessibility of their binding sites. In the composite, the PPI dendrimer introduces additional functional groups that may interact with metal ions, while the MWCNT support provides a carbon-based surface for dendrimer attachment and may facilitate the distribution and accessibility of these functional groups. Using PPI alone could therefore result in a different adsorption capacity, adsorption rate, and separation behavior. Nevertheless, it cannot be concluded from the present data that the free dendrimer would necessarily exhibit lower adsorption performance, since its behavior would depend on factors such as dendrimer generation, concentration, aggregation, functional-group accessibility, solution pH, and the initial metal-ion concentration. The relative contributions of PPI and MWCNTs have not been independently quantified in the present study. A direct experimental comparison among pristine MWCNTs, PPI alone, and the PPI/MWCNT nanocomposite under identical adsorption conditions would be required to establish the contribution of each component. Such experiments should use comparable adsorption conditions and report both metal-ion removal efficiency and equilibrium adsorption capacity. Where appropriate, normalization to the amount of PPI in the composite would also help distinguish the contribution of the dendrimer from that of the nanotube support. Accordingly, the present findings demonstrate the adsorption performance of the PPI/MWCNT composite, but further comparative experiments are needed to determine whether combining PPI with MWCNTs provides a measurable advantage over using PPI alone.

3.6. Effect of Solution Volume on the Reliability of Adsorption Experiments

The solution volume is an important experimental parameter because it determines the liquid-to-solid ratio and may influence mixing efficiency, mass transfer, sampling, and the reliability of concentration measurements. However, a relatively large solution volume does not necessarily increase experimental uncertainty, provided that the adsorbent is uniformly dispersed, the solution is adequately mixed, and representative samples are collected using a consistent procedure. To ensure reliable adsorption measurements, the adsorbent dosage, initial metal-ion concentration, contact time, pH, and sampling procedure should be controlled throughout the experiments. In the present study, the adsorption performance of the PPI/MWCNT nanocomposite was evaluated under optimized conditions, including an adsorbent dosage of 0.06 g/L, an initial metal-ion concentration of 100 mg/L, and a contact time of 20 min. The residual metal-ion concentrations were determined using inductively coupled plasma optical emission spectrometry. Nevertheless, the solution volume alone is insufficient to establish the reliability

or uncertainty of the adsorption results. These aspects should be evaluated based on the experimental procedure, replicate measurements, and analytical quality-control data. Therefore, the solution volume and the associated liquid-to-solid ratio should be explicitly reported to facilitate reproducibility and allow appropriate assessment of the experimental results.

3.7. Adsorption isotherms

Understanding the interaction mechanisms between heavy metal ions and adsorbent surfaces is of critical importance for optimizing adsorption processes and designing efficient treatment systems. In this study, a detailed investigation of adsorption behavior was conducted to provide insight into how Cd^{2+}, Cu^{2+}, and Pb^{2+} ions interact with the PPI/MWCNT nanocomposite surface. By fitting the experimental equilibrium data to these models, it is possible to identify the most appropriate isotherm that accurately represents the adsorption process and to extract critical parameters such as maximum adsorption capacity, adsorption intensity, and binding constants (detailed calculations are provided in the supplementary file). Applying multiple isotherm models not only enables precise characterization of the adsorption process but also provides valuable mechanistic insight, which is necessary for scaling up the treatment system and predicting the performance of PPI/MWCNT in practical heavy metal removal applications. Three models—Langmuir, Freundlich, and Temkin—allow for a comprehensive analysis of adsorption equilibrium, enabling the identification of the dominant adsorption mechanism, whether it is monolayer or multilayer, homogeneous or heterogeneous, and influenced by adsorbate–adsorbent interactions [34–38]. Applying multiple models provides both quantitative parameters, such as adsorption capacity and affinity constants, and qualitative insight into the nature of interactions occurring on the PPI/MWCNT surface.

Table 1 indicated that the Langmuir model provided the highest correlation coefficients (R^2 values) for all three metal ions, indicating that the adsorption process is best described by monolayer adsorption on a homogeneous surface. This observation is consistent with the assumption of the Langmuir isotherm that each adsorption site accommodates only one adsorbate molecule and that there are no interactions between neighboring adsorbed ions. The maximum adsorption capacities ($q_{\square}$) derived from the Langmuir model were found to be 333.3 mg/g for Cd^{2+}, 312.5 mg/g for Cu^{2+}, and 270.0 mg/g for Pb^{2+}, highlighting the excellent adsorption performance of the PPI/MWCNT nanocomposite. In comparison, the Freundlich and Temkin models showed lower correlation coefficients, suggesting that multilayer adsorption and linear decreases in adsorption heat play a lesser role under the experimental conditions. These findings indicate that the PPI/MWCNT surface provides uniform, energetically equivalent adsorption sites that facilitate efficient and selective binding of the heavy metal ions. A graphical representation of the Langmuir isotherm fitting is provided in Fig. 7, where the experimental equilibrium adsorption data closely align with the theoretical Langmuir curves. This further confirms that the adsorption of Cd^{2+}, Cu^{2+}, and Pb^{2+} onto the PPI/MWCNT nanocomposite occurs predominantly via monolayer coverage on homogeneous sites, with strong interaction between the metal ions and functional groups on the dendrimer-modified nanotube surface. These results provide strong evidence for the high adsorption efficiency and well-defined binding behavior of the PPI/MWCNT adsorbent.

Table 1
Adsorption isotherm parameters of metal ions removal by PPI/MWCNT.

Metal	Langmuir				Freundlich			Tempkin		
	Q_0	K_L	R_L	R^2	K_F	n	R^2	B1	K_T	R^2
Cd^{2+}	1620	0.532	0.129	0.999	926	3.78	0.972	280	2.16	0.966
Cu^{2+}	1590	0.598	0.118	0.999	838	3.39	0.983	262	2.93	0.97
Pb^{2+}	1460	0.517	0.185	0.999	769	2.67	0.98	225	2.73	0.968

3.8. Kinetic study

Kinetic studies provide critical insight into the adsorption mechanism. By analyzing kinetic data, one can understand how fast the adsorbate is removed from solution, identify the rate-limiting steps, and optimize operational parameters such as reactor dimensions, adsorbent dosage, and contact time [39, 40]. Understanding the sorption rate is particularly important for designing scalable treatment systems and predicting their performance under real wastewater conditions. By applying these models, it is possible to distinguish between different controlling mechanisms, including surface adsorption, chemical reaction, and intra-particle diffusion, and thereby provide a detailed understanding of the adsorption behavior. Such analysis is essential not only for interpreting the underlying mechanism but also for designing and optimizing practical adsorption systems for efficient heavy metal removal.

The pseudo-first-order (PFO) kinetic model was applied to analyze the experimental adsorption data and evaluate the rate at which heavy metal ions are removed from aqueous solution [41]. This model assumes that the rate of adsorption is directly proportional to the number of unoccupied adsorption sites, making it particularly suitable for describing physisorption processes where interactions are dominated by weak van der Waals forces or electrostatic attraction. By fitting the experimental data to the PFO model, preliminary insight into the overall adsorption rate and its dependence on available surface sites can be obtained. In contrast, the pseudo-second-order (PSO) model indicates a framework for describing adsorption processes controlled by chemisorption, in which the adsorbate forms strong chemical bonds with the adsorbent [42]. This model is particularly relevant for systems in which interactions such as coordination bonding, covalent bonding, or complexation dominate the adsorption process. Importantly, one of the central findings from applying kinetic models is the identification of the rate-limiting step in the adsorption process. In many cases, the adsorption of heavy metal ions onto functionalized adsorbents like PPI/MWCNT is controlled primarily by chemical adsorption, which involves the exchange or sharing of electrons between the adsorbent's active sites (e.g., amine or carboxyl groups) and the metal ions [43, 44]. Recognizing that chemisorption is the rate-limiting step provides critical mechanistic insight, as it indicates that the adsorption capacity and efficiency are strongly dependent on the availability and chemical nature of the surface functional groups, rather than merely on physical diffusion or surface contact.

When the mass transfer of metal ions in the bulk solution surrounding the adsorbent particles is considered negligible, the overall adsorption process can generally be conceptualized as occurring in three sequential steps: (i) the migration of metal ions from the bulk solution to the external surface of the adsorbent, (ii) diffusion of the ions across the boundary layer surrounding the adsorbent particle (often referred to as film or external diffusion), and (iii) intra-particle diffusion, in which ions penetrate into the pores of the adsorbent and occupy internal active sites [45, 46]. Understanding the relative contribution of each of these steps is essential for identifying the rate-controlling mechanism and for optimizing adsorption performance. Among the models used to analyze adsorption kinetics, the intra-particle diffusion (IPD) model is one of the most widely applied for investigating the diffusion-controlled stages of adsorption. The IPD model helps to determine whether the diffusion of adsorbate molecules within the pores of the adsorbent is the limiting step or whether other processes, such as surface adsorption or boundary layer diffusion, dominate the overall rate [47]. Historically, the Weber–Morris equation has been employed as an experimental approach to evaluate intra-particle diffusion. This model expresses the amount of adsorbed species as a function of the square root of contact time, allowing the identification of multi-stage adsorption processes. A linear plot of the adsorbed amount versus the square root of time indicates that intra-particle diffusion contributes significantly to the adsorption mechanism. Deviations from linearity or multi-linear regions typically suggest the simultaneous involvement of multiple mechanisms, such as initial external surface adsorption followed by slower diffusion into the internal pores. Using this approach provides critical insight into the kinetic behavior of heavy metal ions on the PPI/MWCNT adsorbent and helps in elucidating the contributions of different mass transfer processes in the overall adsorption performance.

The kinetic parameters calculated from the experimental adsorption data of Cd^{2+}, Cu^{2+}, and Pb^{2+} onto the PPI/MWCNT nanocomposite are compiled in Table 2 (see supplementary file for detailed calculations). As indicated in Table 2, the R^2 values for the PFO model are relatively low, generally below 0.8 for all three metal ions. This observation suggests that the PFO model, which is typically associated with physisorption processes and assumes that the adsorption rate is proportional to the number of unoccupied sites, does not adequately describe the adsorption behavior of Cd^{2+}, Cu^{2+}, and Pb^{2+} on the PPI/MWCNT nanocomposite. The poor fit implies that physisorption alone is not the dominant mechanism and that other processes, such as chemisorption, play a more significant role. Furthermore, the IPD model was applied to evaluate whether pore diffusion within the adsorbent was a rate-limiting step. The R^2 values obtained for the IPD model are also relatively low, indicating poor linearity and suggesting that intra-particle diffusion does not play a substantial role in controlling the overall adsorption rate. This finding implies that the adsorption of heavy metal ions is not strongly limited by diffusion within the pores of the PPI/MWCNT nanocomposite. Instead, the rapid uptake observed in earlier contact time studies, coupled with the high correlation of the PSO model (discussed in Table 2 and Fig. 8), indicates that chemisorption involving electron sharing or exchange between the metal ions and the functional groups on the PPI/MWCNT surface is likely the dominant adsorption mechanism.Collectively, these kinetic analyses demonstrate that the adsorption of Cd^{2+}, Cu^{2+}, and Pb^{2+} onto PPI/MWCNT is controlled primarily by chemical interactions at the adsorbent surface, rather than

by physical adsorption or intra-particle diffusion. This mechanistic insight is critical for designing efficient adsorption systems and for predicting the performance of the nanocomposite in practical heavy metal removal applications.

Table 2
Investigation of kinetic factors of adsorption of heavy metal ions by PPI/MWCNT.

Metal	$(Q_e)_{Exp}$	PFO			PSO			IPD		
		$(Q_e)_{Cal.}$	k_1	R^2	$(Q_e)_{Cal.}$	k_2	R^2	k_P	I	R^2
Cd^{2+}	1617	1202	0.159	0.983	1620	0.005	0.999	253	912	0.793
Cu^{2+}	1583	1147	0.182	0.99	1590	0.006	0.999	231	869	0.779
Pb^{2+}	1450	1005	0.194	0.988	1460	0.008	0.999	195	793	0.777

3.9. Thermodynamic study

The thermodynamic agents of adsorption provide comprehensive details concerning the nature of the proceeding (Supplementary file). To infer whether the adsorption proceeding is spontaneous or not and also to realize the effect of temperature, thermodynamic studies were utilized considerably [48]. A plot $\ln K_C$ *vs.* (1/T) obtained a straight line, in which ΔS° and ΔH° can be gained from the slope and intercept, respectively. Figure 9 shows the thermodynamics of metal ions removal by PPI/MWCNT. The amounts of thermodynamic agents of Cd^{2+}, $Cu^{2+,}$ and Pb^{2+} adsorption are gathered in Table 3. The endothermic nature of adsorption suggests that higher temperatures favor metal ion uptake, likely by enhancing the mobility of Cd^{2+}, Cu^{2+}, and Pb^{2+} ions in solution and facilitating their interaction with the active sites on the PPI/MWCNT surface. This behavior is consistent with the temperature-dependent adsorption experiments, where higher removal efficiencies were observed at elevated temperatures. The standard entropy change (ΔS°) values are also positive for all three metal ions. This positive ΔS° reflects the strong affinity of the metal ions for the PPI/MWCNT surface, as well as the release of water molecules previously associated with the adsorbent and the solvated metal ions upon binding, which contributes to increased disorder. The standard Gibbs free energy change (ΔG°) is negative for all metal ions. Furthermore, it is observed that ΔG° becomes more negative as the temperature increases, demonstrating that higher temperatures enhance the spontaneity of the adsorption process. Importantly, the magnitude of ΔG° values lies within the range of − 20 to 0 kJ/mol, which is characteristic of physisorption processes [49]. This indicates that, while chemisorption plays a role in specific interactions between functional groups on PPI/MWCNT and metal ions, the overall adsorption mechanism is predominantly driven by physical interactions. The thermodynamic analysis confirms that the adsorption of Cd^{2+}, Cu^{2+}, and Pb^{2+} onto the PPI/MWCNT nanocomposite is spontaneous, endothermic, and driven by favorable entropic changes, with physisorption as the dominant mechanism. These findings provide a strong foundation for understanding the temperature dependence and energetic feasibility of heavy metal removal using the PPI/MWCNT adsorbent.

Table 3
Thermodynamic factors of ion adsorption by PPI/MWCNT.

Metal	ΔH (kJ/mol)	ΔS (J/molK)	ΔG (kJ/mol) at temperatures (K)				
			298	308	318	328	338
Cd^{2+}	3.389	65.061	-3.999	-4.65	-4.3	-5.951	-5.601
Pb^{2+}	6.975	89.658	-6.742	-7.639	-8.536	-8.432	-8.329
Cu^{2+}	4.066	72.809	-5.631	-5.359	-6.087	-6.815	-7.543

3.10. Desorption studies

Over the years, numerous materials have been synthesized and employed to remove pollutants [50–86]. The adsorbent stability, reusability, and regeneration potential are equally important, particularly when considering the practical application of these materials in industrial-scale wastewater treatment. Cost-effectiveness is another key consideration, as adsorbents that can be regenerated and reused multiple times without significant loss of performance are more feasible for real-world implementation. Industrial effluents commonly contain heavy metal ions such as Cd^{2+}, Cu^{2+}, and Pb^{2+}, which necessitate the use of adsorbents capable of not only efficiently removing these contaminants but also sustaining performance over repeated cycles. To evaluate the practical applicability and regenerative capability of the PPI/MWCNT nanocomposite, desorption experiments were conducted under neutral pH conditions (pH = 7). As shown in Fig. 10, the PPI/MWCNT adsorbent exhibited excellent desorption capacity for all three studied metal ions. The desorption efficiencies were found to be 84% for Cd^{2+}, 87% for Cu^{2+}, and 92% for Pb^{2+}. These high desorption values indicate that the PPI/MWCNT nanocomposite allows efficient recovery of adsorbed metal ions and can be regenerated for subsequent adsorption cycles without significant loss of performance. The observed adsorption-desorption behavior demonstrates the strong yet reversible interaction between metal ions and the functional groups on the PPI/MWCNT surface, including amine and carboxyl groups, which facilitate effective binding during adsorption and release under mild conditions during desorption. Such reversible adsorption not only enhances the economic feasibility of the material but also reduces secondary waste generation, making PPI/MWCNT a promising candidate for sustainable and cost-effective heavy metal removal in industrial wastewater treatment [50, 51]. These results highlight that the PPI/MWCNT nanocomposite possesses a desirable combination of high adsorption capacity, thermal and chemical stability, and excellent regeneration ability, which are essential characteristics for practical applications in environmental remediation.

4. Conclusion

In the present study, the adsorption performance of the PPI/MWCNT nanocomposite for the removal of Cd^{2+}, Cu^{2+}, and Pb^{2+} ions from aqueous solutions was systematically investigated and optimized. The results demonstrated that maximum removal efficiency was achieved under the following optimal conditions: adsorbent dosage of 0.06 g/L, initial metal ion concentration of 100 mg/L, and contact time

of 20 min. Under these conditions, the nanocomposite exhibited rapid adsorption kinetics and high removal efficiency for all three heavy metal ions, indicating strong affinity between the adsorbent surface and the target contaminants. Equilibrium studies revealed that the adsorption behavior of Cd^{2+}, Cu^{2+}, and Pb^{2+} was best described by the Langmuir isotherm model, suggesting monolayer adsorption onto a homogeneous surface with finite and energetically equivalent binding sites. The calculated maximum adsorption capacities ($q_{\square}$) were remarkably high, reaching 1620 mg/g for Cd^{2+}, 1590 mg/g for Cu^{2+}, and 1460 mg/g for Pb^{2+}. These values indicate the exceptional adsorption potential of the PPI/MWCNT nanocomposite compared to many conventional adsorbents reported in the literature. Kinetic analysis showed that the adsorption process followed the pseudo-second-order kinetic model, implying that chemisorption is the dominant mechanism governing metal ion uptake. This suggests that electron sharing or exchange occurs between the functional groups of the PPI dendrimer and the heavy metal ions. The abundant amine functional groups present in the PPI structure, combined with the high surface area and conductive network provided by MWCNTs, contribute significantly to the enhanced adsorption performance. The synergistic interaction between PPI and MWCNTs creates a large number of accessible active sites, facilitating rapid mass transfer and efficient metal ion binding. Furthermore, desorption and regeneration experiments demonstrated excellent reusability of the nanocomposite. High desorption efficiencies were achieved over multiple adsorption–desorption cycles, with minimal loss in adsorption capacity. This confirms the structural stability and durability of the PPI/MWCNT nanocomposite under repeated operational conditions, highlighting its practical feasibility for long-term wastewater treatment applications. The combination of high adsorption capacity, rapid uptake kinetics, favorable equilibrium behavior, and outstanding regeneration performance establishes the PPI/MWCNT nanocomposite as a highly efficient and robust adsorbent for toxic heavy metal removal. Its superior performance, coupled with cost-effectiveness and operational stability, underscores its strong potential for sustainable industrial-scale applications in heavy metal remediation and environmental protection.

Declarations

Author Contribution

Bagher Hayati: Methodology, Software, Validation, Formal analysis, Investigation, Data Curation, Writing - Original Draft, Visualization. Mohammad Reza Khodabakhshi: Methodology, Software, Validation, Formal analysis, Investigation, Data Curation, Writing - Original Draft, Visualization. Ramezan Ali Taheri: Conceptualization, Methodology, Software, Validation, Formal analysis, Investigation, Resources, Data Curation, Writing - Original Draft, Writing - Review & Editing, Visualization, Supervision, Project administration, Funding acquisition. Niyaz Mohammad Mahmoodi: Conceptualization, Methodology, Software, Validation, Formal analysis, Investigation, Resources, Data Curation, Writing - Original Draft, Writing - Review & Editing, Visualization, Supervision, Project administration, Funding acquisition

Acknowledgment

Thanks to guidance and advice from "The Clinical Research Development Unit of Baqiyatallah Hospital.

References

1. Fiyadh SS, AlSaadi MA, Jaafar WZ, AlOmar MK, Fayaed SS, Mohd NS, Hin LS, El-Shafie A (2019) Review on heavy metal adsorption processes by carbon nanotubes. J Clean Prod 230:783–793. https://doi.org/https://doi.org/10.1016/j.jclepro.2019.05.154
2. Bilal M, Ihsanullah I, Younas M, Shah MUH (2021) Recent advances in applications of low-cost adsorbents for the removal of heavy metals from water: A critical review. Sep Purif Technol 278:119510
3. Argun ME, Dursun S, Ozdemir C, Karatas M (2007) Heavy metal adsorption by modified oak sawdust: Thermodynamics and kinetics. J Hazard Mater 141:77–85
4. Wang Z, Shen D, Shen F, Wu C, Gu S (2017) Ginkgo biloba L. shells-based adsorbent for the removal of Cu2 + and Cd2 + from aqueous solution: kinetics, isotherm, thermodynamics and mechanisms. J Mol Liq 241:603–611
5. Ajmal M, Khan AH, Ahmad S, Ahmad A (1998) Role of sawdust in the removal of copper (II) from industrial wastes. Water Res 32:3085–3091
6. Li Y-H, Di Z, Ding J, Wu D, Luan Z, Zhu Y (2005) Adsorption thermodynamic, kinetic and desorption studies of Pb2 + on carbon nanotubes. Water Res 39:605–609
7. Hu X, Li Y, Wang Y, Li X, Li H, Liu X, Zhang P (2010) Adsorption kinetics, thermodynamics and isotherm of thiacalix [4] arene-loaded resin to heavy metal ions. Desalination 259:76–83
8. Sadeek SA, Negm NA, Hefni HHH, Wahab MMA (2015) Metal adsorption by agricultural biosorbents: adsorption isotherm, kinetic and biosorbents chemical structures. Int J Biol Macromol 81:400–409
9. Nasernejad B, Zadeh TE, Pour BB, Bygi ME, Zamani A (2005) Camparison for biosorption modeling of heavy metals (Cr (III), Cu (II), Zn (II)) adsorption from wastewater by carrot residues. Process Biochem 40:1319–1322
10. Marković S, Stanković A, Lopičić Z, Lazarević S, Stojanović M, Uskoković D (2015) Application of raw peach shell particles for removal of methylene blue. J Environ Chem Eng 3:716–724
11. Iijima S (1991) Helical microtubules of graphitic carbon. Nature 354:56–58
12. Li Y-H, Wang S, Luan Z, Ding J, Xu C, Wu D (2003) Adsorption of cadmium (II) from aqueous solution by surface oxidized carbon nanotubes. Carbon N Y 41:1057–1062
13. Li Y-H, Wang S, Cao A, Zhao D, Zhang X, Xu C, Luan Z, Ruan D, Liang J, Wu D (2001) Adsorption of fluoride from water by amorphous alumina supported on carbon nanotubes. Chem Phys Lett 350:412–416
14. You J, Zhao Y, Wang L, Bao W, He Y (2020) Atomic layer deposition of γ-Fe2O3 nanoparticles on modified MWCNT for efficient adsorption of Cr (VI) ions from aqueous solution. J Phys Chem Solids 142:109441

15. Yu X-Y, Luo T, Zhang Y-X, Jia Y, Zhu B-J, Fu X-C, Liu J-H, Huang X-J (2011) Adsorption of lead (II) on O_2-plasma-oxidized multiwalled carbon nanotubes: thermodynamics, kinetics, and desorption. ACS Appl Mater Interfaces 3:2585–2593
16. Eskandarian L, Arami M, Pajootan E (2014) Evaluation of adsorption characteristics of multiwalled carbon nanotubes modified by a poly(propylene imine) dendrimer in single and multiple dye solutions: Isotherms, kinetics, and thermodynamics. J Chem Eng Data 59:444–454. https://doi.org/10.1021/je400913z
17. Ghasempour A, Pajootan E, Bahrami H, Arami M (2017) Introduction of amine terminated dendritic structure to graphene oxide using Poly (propylene Imine) dendrimer to evaluate its organic contaminant removal. J Taiwan Inst Chem Eng 71:285–297
18. Mehra NK, Jain NK (2016) Multifunctional hybrid-carbon nanotubes: new horizon in drug delivery and targeting. J Drug Target 24:294–308
19. Mahmoodi NM, Sadeghi U, Maleki A, Hayati B, Najafi F (2014) Synthesis of cationic polymeric adsorbent and dye removal isotherm, kinetic and thermodynamic. J Ind Eng Chem 20:2745–2753
20. Mohamed A, Yousef S, Abdelnaby MA, Osman TA, Hamawandi B, Toprak MS, Muhammed M, Uheida A (2017) Photocatalytic degradation of organic dyes and enhanced mechanical properties of PAN/CNTs composite nanofibers. Sep Purif Technol 182:219–223
21. Murugan E, Arumugam S, Panneerselvam P (2016) New nanohybrids from poly (propylene imine) dendrimer stabilized silver nanoparticles on multiwalled carbon nanotubes for effective catalytic and antimicrobial applications. Int J Polym Mater Polym Biomater 65:111–124
22. Murugan E, Arumugam S (2014) New dendrimer functionalized multi-walled carbon nanotube hybrids for bone tissue engineering. RSC Adv 4:35428–35441
23. Hayati B, Maleki A, Najafi F, Rezaee R, Puttaiah SH, Marzban N, McKay G (2020) PPI/CNT nanocomposite for novel high capacity removal of the toxic heavy metals, Hg, Pb and Ni from water, Desalin. Water Treat 198:190–199
24. Souza Filho AG, Jorio A, Samsonidze GG, Dresselhaus G, Saito R, Dresselhaus MS (2003) Raman spectroscopy for probing chemically/physically induced phenomena in carbon nanotubes. Nanotechnology 14:1130
25. Rathod V, Tripathi R, Joshi P, Jha PK, Bahadur P, Tiwari S (2019) Paclitaxel encapsulation into dual-functionalized multi-walled carbon nanotubes. AAPS PharmSciTech 20:1–13
26. Hoa LTM (2018) Characterization of multi-walled carbon nanotubes functionalized by a mixture of HNO_3/H_2SO_4, Diam. Relat Mater 89:43–51
27. Murugan E, Vimala G (2011) Effective functionalization of multiwalled carbon nanotube with amphiphilic poly (propyleneimine) dendrimer carrying silver nanoparticles for better dispersability and antimicrobial activity. J Colloid Interface Sci 357:354–365
28. Chen D, Shi F, Xu W, Shen H, Zhu Y (2021) A simultaneous extraction and enrichment method for rapid detection of polar chlorophenoxy acid and non-steroidal anti-inflammatory drugs from

wastewater based on low-generation dendrimer poly(propylene imine). Microchem J 168:106454. https://doi.org/10.1016/j.microc.2021.106454

29. Chen Q, Peng Q, Zhao X, Sun H, Wang S, Zhu Y, Liu Z, Wang C, He X (2020) Grafting carbon nanotubes densely on carbon fibers by poly (propylene imine) for interfacial enhancement of carbon fiber composites. Carbon N Y 158:704–710
30. He X, Liu G, Yan B, Suo H, Zhao C (2016) Significant enhancement of electrochemical behaviour by incorporation of carboxyl group functionalized carbon nanotubes into polyaniline based supercapacitor. Eur Polym J 83:53–59
31. Akbari H, Gholami M, Akbari H, Adibzadeh A, Taghavi L, Hayati B, Nazari S (2020) Poly (amidoamine) generation 6 functionalized Fe_3O_4@SiO_2/GPTMS core–shell magnetic NPs as a new adsorbent for Arsenite adsorption: kinetic, isotherm and thermodynamic studies. J Environ Heal Sci Eng 18:253–265. https://doi.org/10.1007/s40201-020-00461-4
32. Priya AK, Yogeshwaran V, Rajendran S, Hoang TKA, Soto-Moscoso M, Ghfar AA, Bathula C (2022) Investigation of mechanism of heavy metals (Cr^{6+}, Pb^{2+} & Zn^{2+}) adsorption from aqueous medium using rice husk ash: Kinetic and thermodynamic approach. Chemosphere 286:131796
33. Lakshmipathy R, Sarada NC (2015) A fixed bed column study for the removal of Pb^{2+} ions by watermelon rind. Environ Sci Water Res Technol 1:244–250
34. Thajeel AS (2013) Isotherm, kinetic and thermodynamic of adsorption of heavy metal ions onto local activated carbon. Aquat Sci Technol 1:53–77
35. Do DD (1998) Adsorption analysis: Equilibria and kinetics (with cd containing computer MATLAB programs). World Scientific
36. Surchi KMS (2011) Agricultural wastes as low cost adsorbents for Pb removal: kinetics, equilibrium and thermodynamics. Int J Chem 3:103
37. Tan IAW, Ahmad AL, Hameed BH (2008) Adsorption of basic dye using activated carbon prepared from oil palm shell: batch and fixed bed studies. Desalination 225:13–28
38. Dada AO, Ojediran JO, Okunola AA, Dada FE, Lawal AI, Olalekan AP, Dada O (2019) Modeling of biosorption of Pb (II) and Zn (II) ions onto PaMRH: Langmuir, Freundlich, Temkin, Dubinin-Raduskevich, Jovanovic, Flory-Huggins, Fowler-Guggenheim and Kiselev comparative isotherm studies. Int J Mech Eng Technol 10:1048–1058
39. Boulaiche W, Hamdi B, Trari M (2019) Removal of heavy metals by chitin: equilibrium, kinetic and thermodynamic studies. Appl Water Sci 9:1–10
40. Indhumathi P, Sathiyaraj S, Koelmel JP, Shoba SU, Jayabalakrishnan C, Saravanabhavan M (2018) The efficient removal of heavy metal ions from industry effluents using waste biomass as low-cost adsorbent: thermodynamic and kinetic models. Z Für Phys Chemie 232:527–543
41. Hsieh W-H, Chiu W-T, Lee Y-S, Ho Y-S (2004) Bibliometric analysis of patent ductus arteriosus treatments. Scientometrics 60:105–215

42. Lu N, Hu T, Zhai Y, Qin H, Aliyeva J, Zhang H (2020) Fungal cell with artificial metal container for heavy metals biosorption: Equilibrium, kinetics study and mechanisms analysis. Environ Res 182:109061
43. Tan IAW, Ahmad AL, Hameed BH (2009) Adsorption isotherms, kinetics, thermodynamics and desorption studies of 2,4,6-trichlorophenol on oil palm empty fruit bunch-based activated carbon. J Hazard Mater 164:473–482
44. Iram M, Guo C, Guan Y, Ishfaq A, Liu H (2010) Adsorption and magnetic removal of neutral red dye from aqueous solution using Fe3O4 hollow nanospheres. J Hazard Mater 181:1039–1050. https://doi.org/https://doi.org/10.1016/j.jhazmat.2010.05.119
45. Keskinkan O, Goksu MZL, Yuceer A, Basibuyuk M, Forster CF (2003) Heavy metal adsorption characteristics of a submerged aquatic plant (Myriophyllum spicatum), Process Biochem. 39 179–183
46. Paul S, Bera D, Chattopadhyay P, Ray L (2006) Biosorption of Pb (II) by Bacillus cereus M1 16 immobilized in calcium alginate gel. J Hazard Subst Res 5:2
47. Weber WJ Jr, Morris JC (1963) Kinetics of adsorption on carbon from solution. J Sanit Eng Div 89:31–59
48. Özsin G, Kılıç M, Apaydın-Varol E, Pütün AE (2019) Chemically activated carbon production from agricultural waste of chickpea and its application for heavy metal adsorption: equilibrium, kinetic, and thermodynamic studies. Appl Water Sci 9:1–14
49. Gerçel Ö, Özcan A, Özcan AS, Gercel HF (2007) Preparation of activated carbon from a renewable bio-plant of Euphorbia rigida by H2SO4 activation and its adsorption behavior in aqueous solutions. Appl Surf Sci 253:4843–4852
50. Ezeonuegbu BA, Machido DA, Whong CMZ, Japhet WS, Alexiou A, Elazab ST, Qusty N, Yaro CA, Batiha GE-S (2021) Agricultural waste of sugarcane bagasse as efficient adsorbent for lead and nickel removal from untreated wastewater: Biosorption, equilibrium isotherms, kinetics and desorption studies. Biotechnol Rep 30:e00614
51. Morosanu I, Teodosiu C, Paduraru C, Ibanescu D, Tofan L (2017) Biosorption of lead ions from aqueous effluents by rapeseed biomass. N Biotechnol 39:110–124
52. Abdelmobdy M, Gomaa H, Sanad MMS, Shenashen MA, Kotb A, Nagiub A (2025) Silver nanowires/chitosan-derived porous carbon sheets nanocomposite for the efficient removal of crystal violet and methylene blue dyes from wastewater. Inorg Chem Commun 174:114041
53. Moyo S, Mahlangu OT, Vilakati GD, Mamba BB, De Kock LA, Gumbi NN, Nxumalo EN (2025) MOF incorporated Polyethersulfone/Polylactic Acid ultrafiltration membranes for the catalytic removal of dyes via persulfate activation. Inorg Chem Comm 171:113634
54. Thottathil S, Puttaiahgowda YM, Selvaraj R, Elambalassery JG, Vinayagam R, Varadavenkatesan T (2025) Experimental and DFT studies of Congo red and AB 113 dyes removal by adsorption and disinfection using novel triazine-based porous organic polymer. J Mol Liq 429:127628

55. Sarkar S, Mukherjee S, Saha A, Bhowal A, Das P (2025) Functionalized MXene nanosheets for efficient Safranin dye removal from aqueous solution: A batch study and RSM optimized parameters. Surf Interfaces 68:106636
56. Aziz KHH, Mustafa FS, Hamarawf RF, Omer KM (2025) Adsorptive removal of toxic heavy metals from aquatic environment by metal organic framework (MOF): A review. J Water Process Eng 70:106867
57. Matheen IA, Raza AA, Aatif AM, Ravi S, Kubaib A, Majeed SA, Ahmed SZ, Tajudeen SS (2025) Enhanced photocatalytic degradation of organic contaminants using a novel bimetallic Ag-Cu doped biphenyl linked covalent triazine framework: Experimental, theoretical and toxicological assessments. J Photochem Photobiol Chem 462:116264
58. Zaamouchi I, Kaci MM, Zidane Y, Belaid S, Bouacida S, Benmerad B (2024) The impressive photocatalytic performance of Zn-MOF as a novel photocatalyst for the effective purification of dyes under solar exposure. J Mol Struct 1299:137070
59. Hacıefendioğlu D, Polat M, Özel S, Çelikbıçak Ö, Tuncel A (2025) A porphyrinic, titanium based metal organic framework as a superior photocatalyst for visible light driven dye degradation: Fast and almost complete degradation with high initial Rhodamine B concentration. Surf Interfaces 58:105778
60. Naseer M, Nazir S, Kausar A, Rashid MA, Usman M, Naseer R, Iqbal J (2025) Enhanced removal of cationic dyes using copper-based MOF-graphene oxide composite: Synthesis, characterization and performance evaluation. Chem Eng Sci 307:121362
61. Han L, Liu J, Li F, Zhao Y, Guo X, Wang S, Ji Z (2025) CoMn-MOF-74 coated ceramic membranes for catalytic ozonation of azo dye in wastewater by membrane dispersion - membrane catalysis process. J Environ Chem Eng 13:116612
62. Liu P, Lyu J, Bai P (2025) Synthesis of mixed matrix membrane utilizing robust defective MOF for size-selective adsorption of dyes. Sep Purif Technol 354:128672
63. Yan YT, Fan XD, Lu JL, Yang ZH, Zhang YB, Wu YL, Zhang WY, Wang YY (2025) A novel porous Zn-MOF based on binuclear metal clusters for fluorescence detection of Cr(VI) and adsorption of dyes. J Mol Struct 1322:140553
64. Cheng S, Li Y, Yu Z, Su Y (2025) Efficient adsorption removal of anionic dyes by waste PET-derived MIL-101(Cr). Sep Purif Technol 354:128985
65. Song R, Han W, Yang Z, Ye Z, Yang Y, Zheng H, Zhao S, Zeng G (2025) Mixed matrix membranes (MMMs) for dyes and antibiotics removal from wastewater using photo-Fenton catalysis MOFs as additives. J Water Process Eng 69:106614
66. Mukhtiar S, Rauf S, Ibrahim MM, Ullah H, Shehzad FK, Nadeem M, Asif HM, Hussain S, Saleem U (2025) Harnessing encapsulated polyoxometalate in MOFs for sonophotocatalytic Cr(VI) reduction: Unveiling the pathway to eco-friendly chromium remediation. J Photochem Photobiol Chem 468:116506

67. Plesner TJ, Wang F, Ouyang Y, Khazaee Z, Zhou P, Zhang M, Eser BE, Zhang Y, Guo Z (2025) Cooperative action from Cu-centered MOF and a laccase for enhanced decolorization of synthetic dyes. Biochem Eng J 221:109807
68. Thamer BM, Al-aizari FA, Abdo HS, El-Newehy MH (2025) Upcycling polystyrene foam waste into highly efficient MOF(Cr)-incorporated fiber composite adsorbent to rid water of hazardous dyes. Chem Eng Sci 311:121636
69. Sharma P, Sharma M, Nimesh D, Gupta R (2025) Exploring the potential of hydrogel adsorbents for antibiotic removal from water: A review. J Mol Liq 426:127383
70. Arshad Z, Tanimu A, Alhooshani K, Ali SA (2025) A dual-purpose β-cyclodextrin-derived sorbent decorated with chelating residues of aminomethylphosphonate and aspartic acid for removal of polyaromatic hydrocarbons and toxic metal ions. J Mol Liq 426:127500
71. Houda Douba O, Mohammedi M, Fizir S, Sabour M, Bidaoui F, Zermane B, Cheknane (2025) Porous sodium alginate/MCM-41 composites for malachite green removal from aqueous medium: Kinetic, isotherm, and mechanism study. J Mol Liq 427:127402
72. Mubarak AA, Ilyas RA, Ngadi N, Nordin AH, Alkbir MFM (2025) Surface functionalization of nanocellulose with polyethyleneimine and magnetic nanoparticles for efficient removal of anionic dye in wastewater. Int J Biol Macromol 318:145205
73. Shukla AK, Alam J, Alhoshan M (2025) Trimesoyl chloride crosslinked chitosan: An efficient adsorbent for Congo red dye removal from water - kinetic and isotherm analysis. Int J Biol Macromol 319:145538
74. Rezaei A, Taheri RA, Rahimi-Nasrabadi M, Mirzaei M (2025) Innovative electro-Fenton approach: Co-NC/FeTiO3 for enhanced diazinon removal from wastewater. Mater Chem Phys 334:130461
75. Barahimi V, Taheri RA, Mazaheri A et al (2020) Fabrication of a novel antifouling TiO2/CPTES/metformin-PES nanocomposite membrane for removal of various organic pollutants and heavy metal ions from wastewater. Chem Pap 74:3545–3556. https://doi.org/10.1007/s11696-020-01178-2
76. Khansary MA, Mellat M, Saadat SH, Fasihi-Ramandi M, Kamali M, Taheri RA (2017) An enquiry on appropriate selection of polymers for preparation of polymeric nanosorbents and nanofiltration/ultrafiltration membranes for hormone micropollutants removal from water effluents. Chemosphere 168:91–99
77. Rabeie B, Mahmoodi NM (2025) Green synthesis of biopolymer-driven dual functional carboxymethyl cellulose composite (CMC/MIL100 (Fe)/MIL88A (Al)) as a Z-scheme photocatalyst and an adsorbent for water pollutants. Int J Biol Macromol 329:147358
78. Talebipour S, Panahi PN, Mahmoodi NM, Rasoulifard MH, Rabeie B (2025) Novel eco-friendly MIL-88B/ZIF-67 hybrid composites for the efficient degradation of Direct Red 23 from wastewater under visible light irradiation. J Mol Liq 439:128873
79. Rabeie B, Mahmoodi NM (2025) Environmentally friendly novel covalent organic framework composites as porous photocatalysts and adsorbents for Tetracycline and dyes (Congo Red and

Methylene Blue) removal: Green synthesis, kinetics, regeneration, and removal mechanisms. Appl Mater Today 46:102884

80. Rabeie B, Mahmoodi NM (2026) Rational design of a COF/MIL-100 hybrid for synergistic photocatalytic–adsorptive removal of persistent pollutants and techno-economic assessment. Appl Mater Today 52:103418
81. Rabeie B, Mahmoodi NM (2025) Fish scales-like magnetic covalent organic framework (COF) composite: Synthesis and photocatalytic tetracycline and dye degradation using LED visible light in water. Surf Interfaces 72:107251
82. Rabeie B, Mahmoodi NM, Mahkam M (2022) Morphological diversity effect of graphene quantum dot/MIL88A (Fe) composites on dye and pharmaceuticals (tetracycline and doxycycline) removal. J Environ Chem Eng 10(5):108321
83. Rabeie B, Mahkam M, Mahmoodi NM, Lan CQ (2021) Graphene quantum dot incorporation in the zeolitic imidazolate framework with sodalite (SOD) topology: Synthesis and improving the adsorption ability in liquid phase. J Environ Chem Eng 9(6):106303
84. Rabeie B, Mahmoodi NM (2024) Green and environmentally friendly architecture of starch-based ternary magnetic biocomposite (Starch/MIL100/$CoFe_2O_4$): Synthesis and photocatalytic degradation of tetracycline and dye. Int J Biol Macromol 274:133318
85. Rabeie B, Mahmoodi NM, Kazemian H (2026) Visible light assisted magnetic COF/HKUST/$CoFe_2O_4$ composite as a novel photocatalyst: Green synthesis and efficient degradation of pollutants (dye and pharmaceutical) in water. Adv Compos Hybrid Mater 9:160
86. Mahmoodi NM, Mahmoodi B, Hoseinzadeh H et al (2026) Room temperature synthesized PVA/GO/ZIF-67 ternary nanocomposite as a high-performance multifunctional adsorbent for malachite green and tetracycline removal. Chem Pap. https://doi.org/10.1007/s11696-026-05210-9

Figures

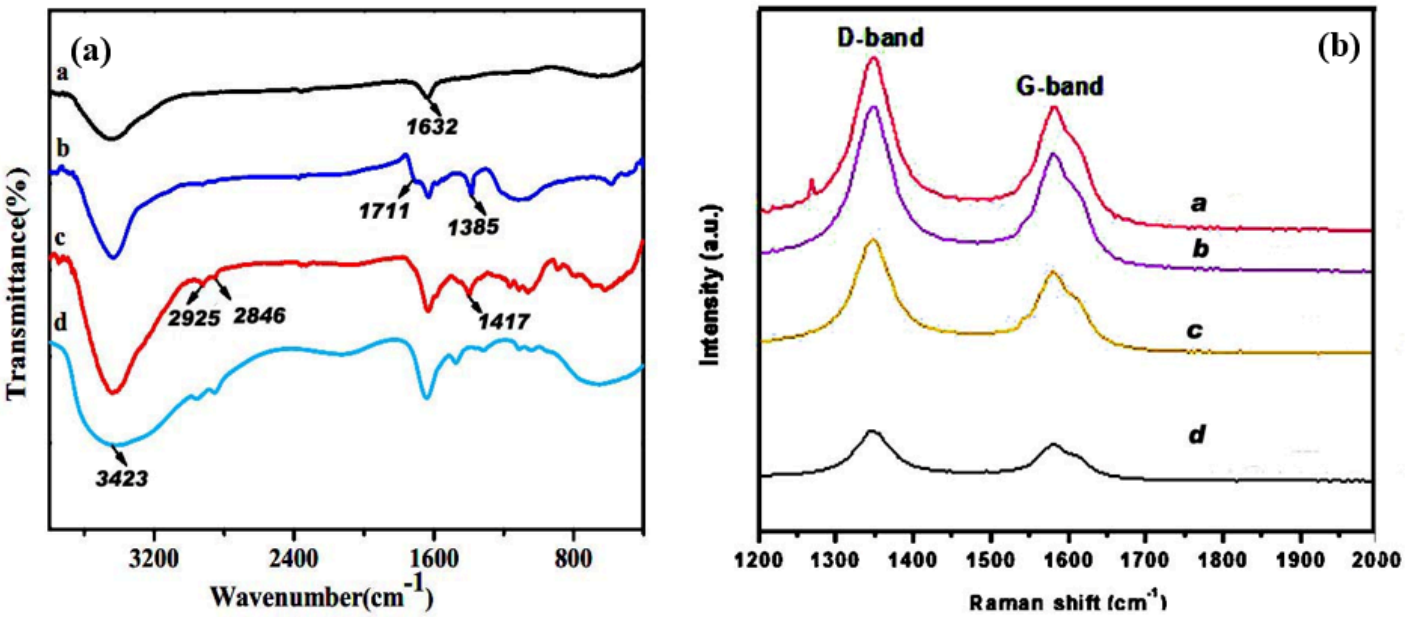


Figure 1

(a) FT-IR and (b) Raman spectra of as-constructed samples (a: MWCNT, b: MWCNT-COOH, c: MWCNT-COCl, and d: PPI/MWCNT).

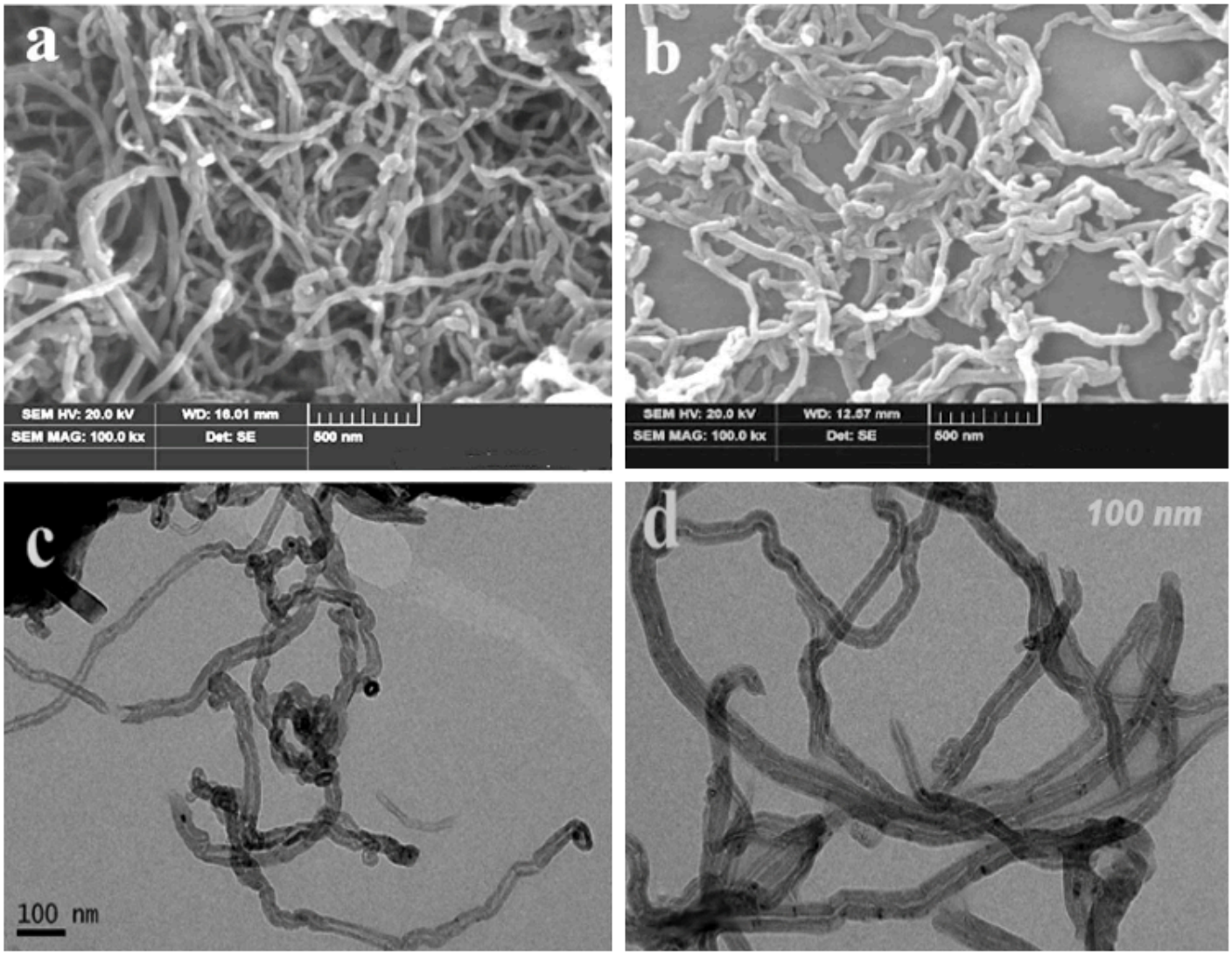


Figure 2

The SEM images of (a) MWCNT-COOH and (b) PPI/MWCNT samples. The TEM images of (c) MWCNT-COOH and (d) PPI/MWCNT samples.

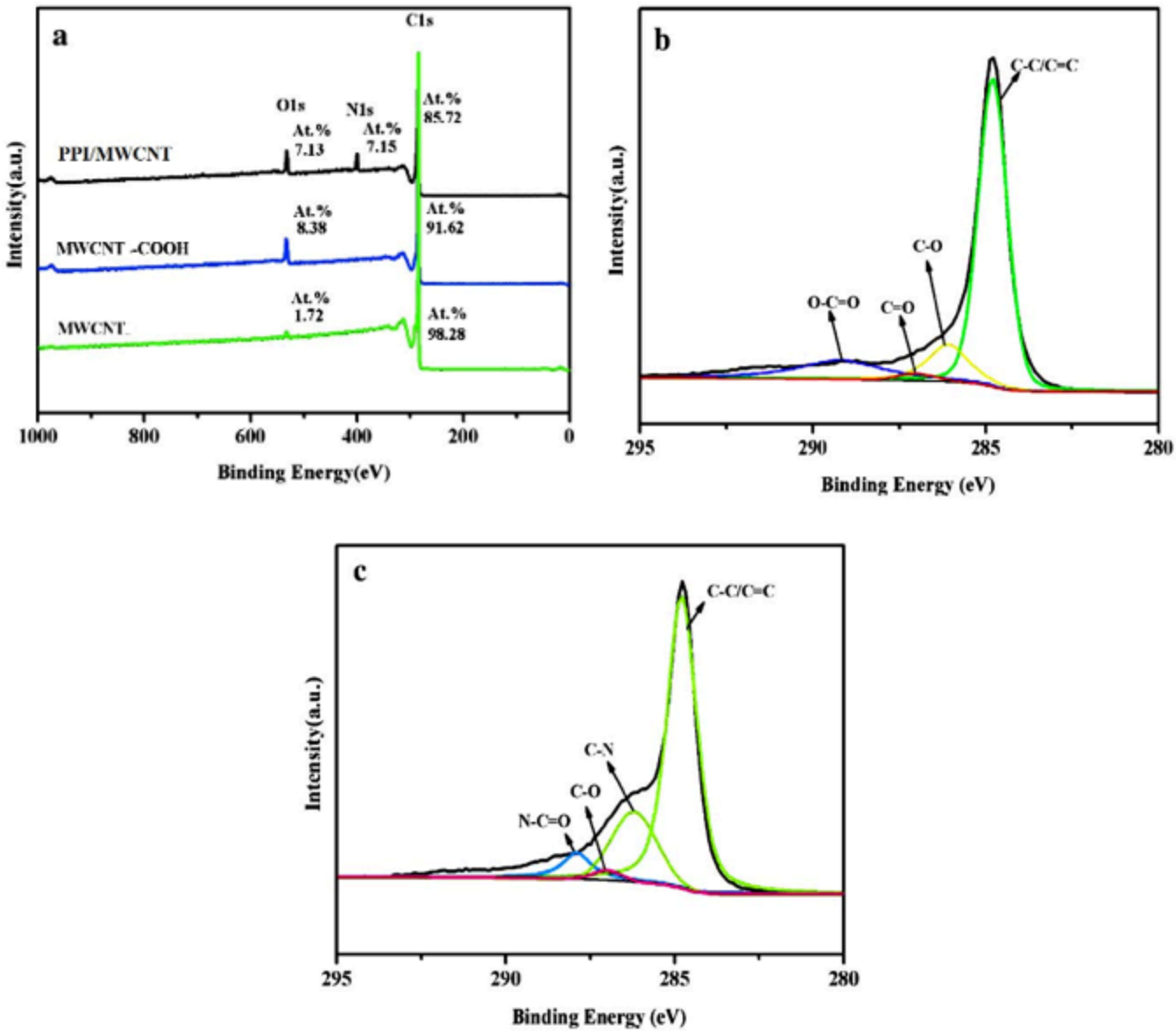


Figure 3

(a) The survey XPS spectrum of as-constructed samples, high-resolution scans of C1s for (b) MWCNT-COOH and (c) PPI/MWCNT samples.

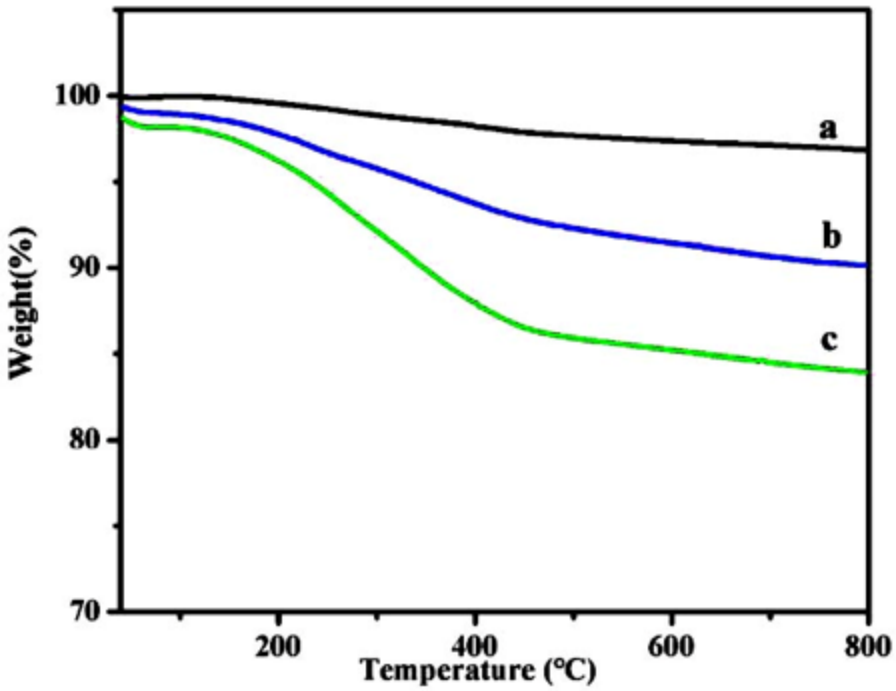


Figure 4

TGA plots of (a) MWCNT, (b) MWCNT-COOH, and (c) PPI/MWCNT samples.

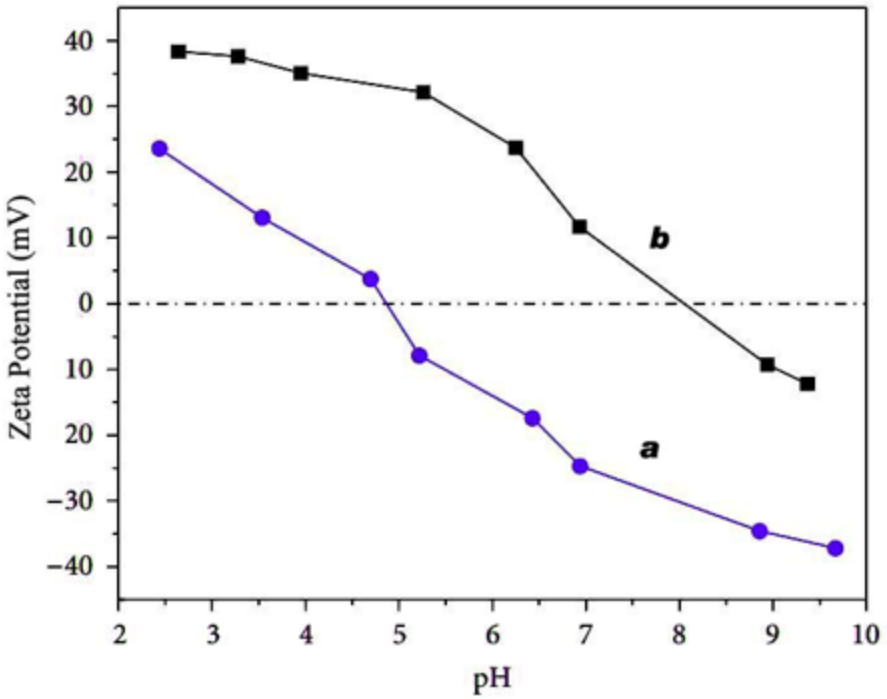


Figure 5

Zeta potential of (a) MWCNT and (b) PPI/MWCNT samples.

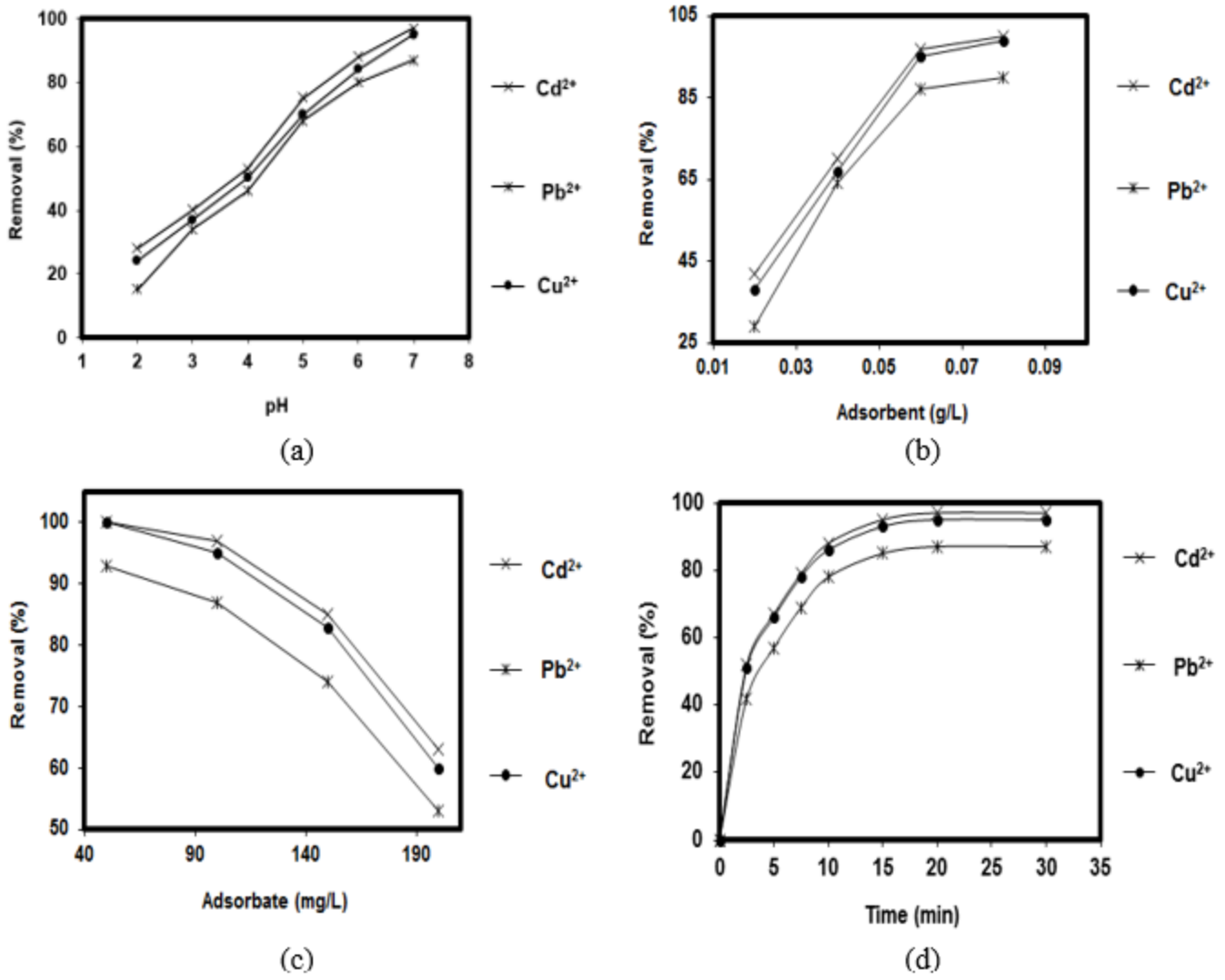


Figure 6

Influence of (a) pH, (b) adsorbent dosage, (c) adsorbate concentrations, and (d) contact time on elimination of Cd^{2+}, Cu^{2+} and Pb^{2+} by PPI/MWCNT system.

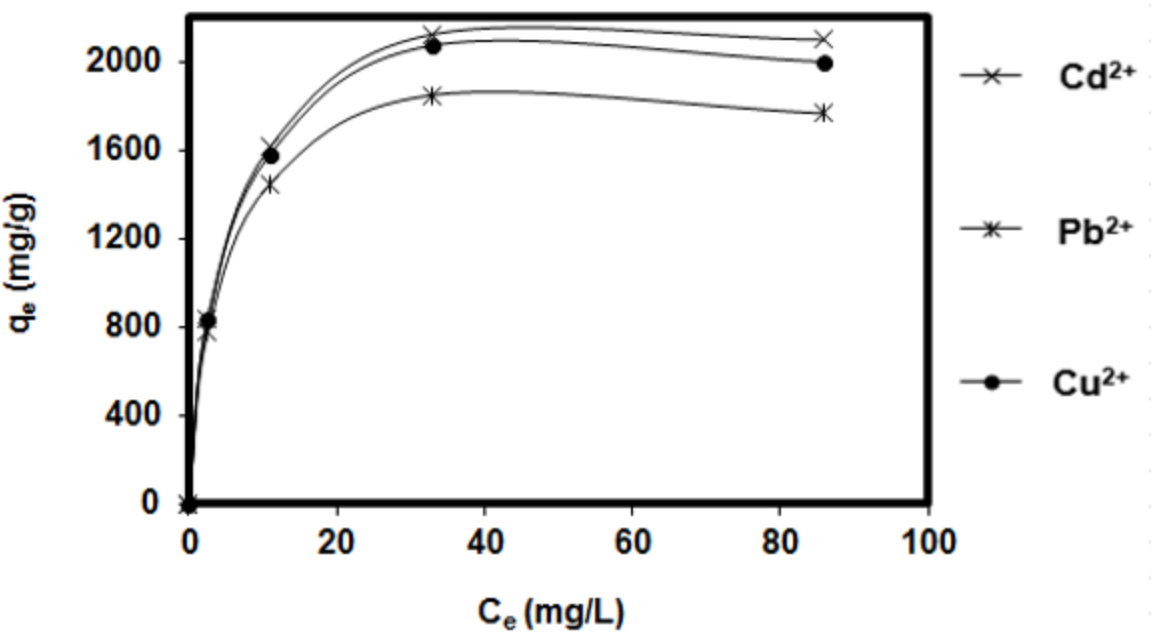


Figure 7

Langmuir isotherm of heavy metal ions adsorption on PPI/MWCNT system.

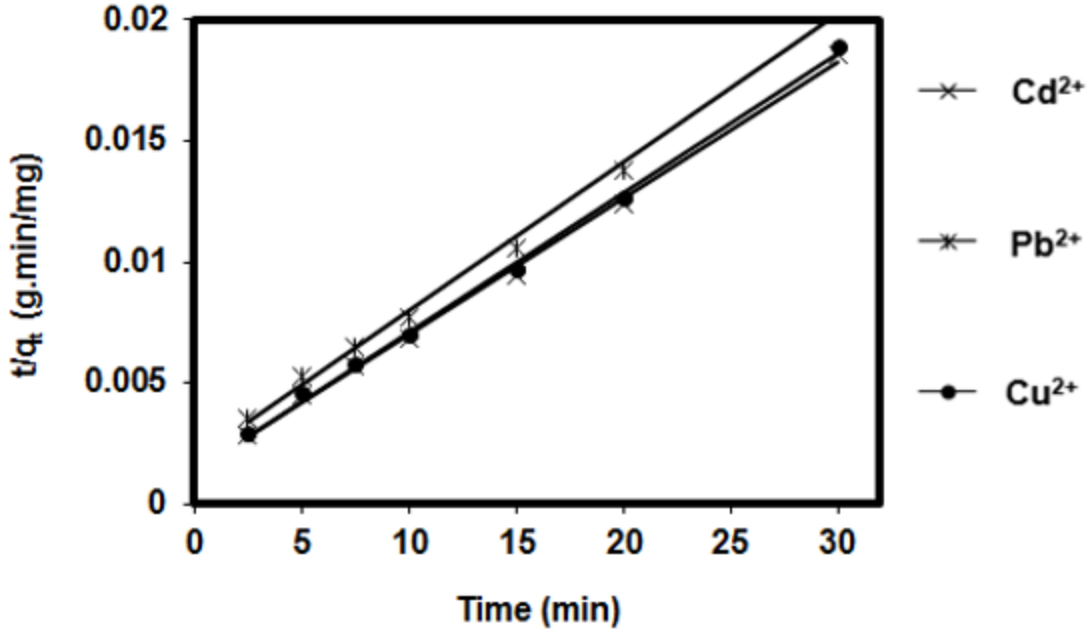


Figure 8

The PSO rate model for adsorption of heavy metal ions by PPI/MWCNT.

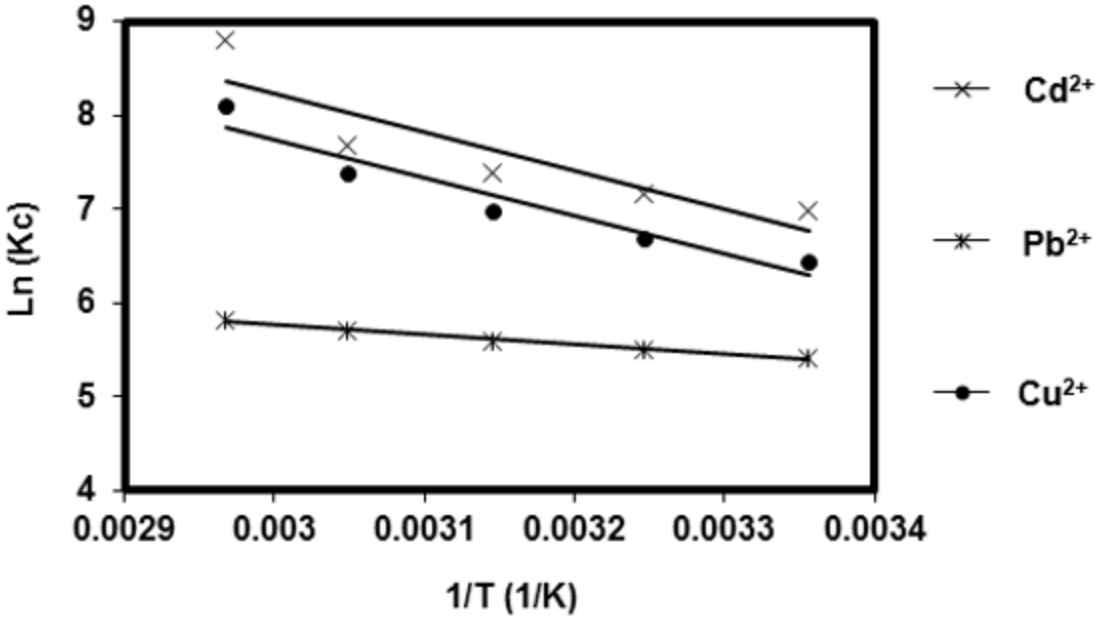


Figure 9

lnK_c *vs.* 1/T plot (Van't Hoff plot) for ion adsorption on the PPI/MWCNT.

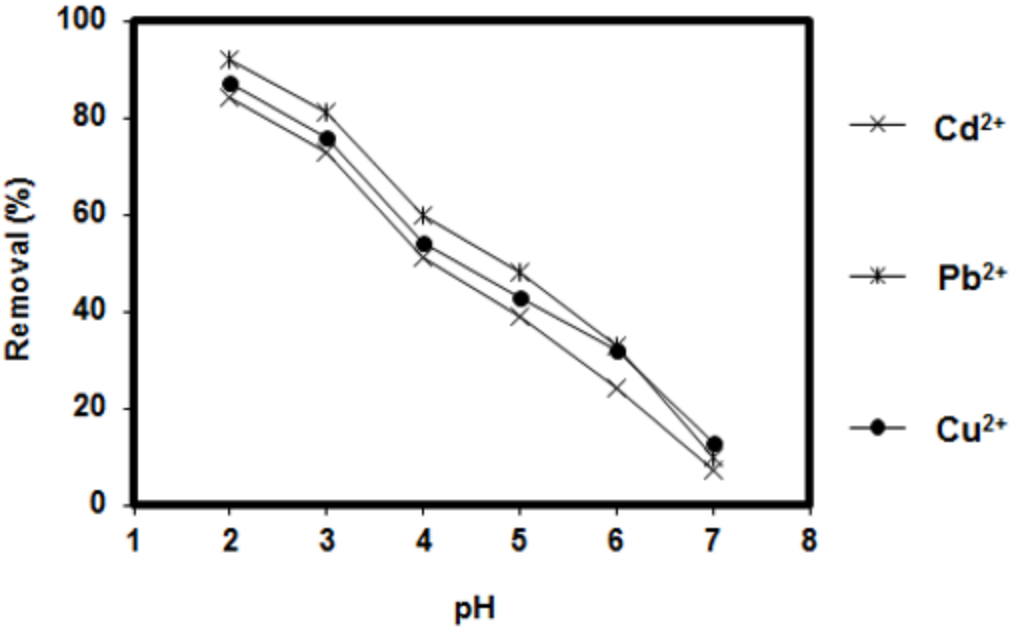


Figure 10

Desorption of heavy metal ions on the surface of PPI/MWCNT.

Supplementary Files

This is a list of supplementary files associated with this preprint. Click to download.

- Supplementaryfile.docx